Eur. Phys. J. Plus (2021) 136:1147
https://doi.org/10.1140/epjp/s13360-021-02091-7

THE EUROPEAN PHYSICAL JOURNAL PLUS

Regular Article

Effect of Ga excess concentration on the structural, electronic, magnetic, elastic and thermoelectric properties of $Fe_{2-x}NiGa_{1+x}$ Heusler alloys: results of FP-LAPW calculations

S. Chami[1,2,a], **S. Lamari**[1,2], **Z. Charifi**[3,4]

[1] Department of Physics, Faculty of Science, University Ferhat Abbas Setif 1, 19000 Setif, Algeria
[2] Laboratoire dEtude Des Surfaces Et Interfaces Des Matériaux Solides, University Ferhat Abbas Setif 1, 19000 Setif, Algeria
[3] Department of Physics, Faculty of Science, University of Msila, 28000 Msila, Algeria
[4] Laboratory of Physics and Chemistry of Materials, University of Msila, Msila, Algeria

Received: 20 July 2021 / Accepted: 18 October 2021

Abstract The structural, electronic, magnetic, elastic and thermoelectric properties of $Fe_{2-x}NiGa_{1+x}$ ($x = 0, 0.25, 0.5, 0.75, 1$) Heusler alloys are investigated through ab initio calculations based on density functional theory (DFT) within the full potential linearized augmented plane wave (FP-LAPW) method. After substituting Fe by Ga in the unit cell, we find that the composition dependence of both the lattice constants and bulk modulii are not monotonous. Moreover, while these alloys still keep their metallic character, the calculated electronic structure shows an increase in the p–d and a corresponding decrease in the d–d orbital hybridizations between the transition metal and the main group elements. The distribution of the spin magnetic moments shows that these materials are ferromagnetic with their respective magnetic moments and Curie temperatures decreasing linearly with the Ga excess concentration x. The $Fe_{2-x}NiGa_{1+x}$ Heusler alloys ($x = 0, 0.25, 0.5, 0.75, 1$) we studied, are all found to be mechanically stable and, because of their high B/G ratio, ductile. The BoltzTraP code is used to assess the influence of Fe substitution by Ga on the transport properties. The Seebeck coefficient, electrical conductivity, thermal conductivity and figure of merit for the $Fe_{2-x}NiGa_{1+x}$ alloy are all calculated.

1 Introduction

From a fundamental point of view, full and half Heusler compounds have up till now been studied quite extensively [1–3]. These materials have versatile properties that are very much sought after in different applications such as in the fabrication of new magnets [4] and spin valves as is the case in some devices [5]. Due to their half-metallic ferromagnetic properties, these compounds are destined to play an important role in the emerging field of spintronics [6–10]. In connection with the important issue of spin injection in these kinds of applications, among the best candidates are materials that are metallic for electrons of

[a] e-mail: sachami_dz@yahoo.fr (corresponding author)

one spin orientation and semiconducting for electrons of the other spin direction. Moreover, alongside their fascinating magnetic and transport properties, the thermoelectric properties of this large class of materials is at least as attractive and many research groups have in fact invested a large effort in improving their thermoelectric performances [11–17].

Historically, the interest in these compounds goes back to 1903 when F. Heusler, a German mining engineer and chemist, discovered ferromagnetism in Cu_2MnAl even though none of its constituents by itself makes a magnetic material [18, 19]. These Heusler compounds, as they came to be called, are characterized by their ability to have their valence electron concentration varied through the partial substitution of elements, the properties however still remain very crystal structure dependent [18, 20]. In general, the fully ordered Heusler compounds X_2YZ, X and Y being transition metal elements and Z a main group one, crystallize in the cubic L_{21} structure [21, 22]. However, many of the Heusler compounds synthesized to date are found to crystallize either in the partially disordered B_2 phase where half of the Y and Z atoms interchange their positions or the fully disordered A_2 one where the X, Y and Z atoms are randomly distributed over all available lattice sites whereby they lose their half-metallic character[23–26].

Heusler alloys form an interesting class of materials because they offer the possibility of investigating lattice atomic ordering and magnetic coupling for intermetallic compounds [27]. With Z being a main group element, the Fe_2-based Heusler alloys Fe_2CrZ [28, 29] and Fe_2MnZ [30, 31] have been shown to exhibit very interesting magnetic structure and magnetic martensitic transformation shape memory properties. However, for spintronic applications, due to their high Curie temperature, spin polarization and magnetic moment [32], Co_2-based compounds have so far been explored the most [33–38].

Fe_2NiZ (Z = Al, Ga, Si and Ge) Heusler alloys were synthesized and investigated systematically [39]. In addition to that, the Heusler compounds $NiMnGa_2$ and $CoMnGa_2$, i.e., of the form XYZ_2 have also been reported in Refs. [40] and [41], respectively, where, due to their richer composition in the main group element Z, stronger covalent bonding is found.

Heusler compounds with the chemical formula XYZ_2 such as $NiMnGa_2$ [40] and $CoMnGa_2$ [41, 42] have been investigated too. These materials are characterized by their strong covalent bonding arising from their Z-rich composition. In these systems, when the structure changes from Hg_2CuTi-type Mn_2CoGa to Cu_2MnAl-type $CoMnGa_2$, the gradual replacement of Mn atoms by new Ga atoms will change the role of the main atom that is responsible for magnetism and in fact Li et al. [43] point out in their work to unusual lattice constant changes and a concomitant tunable magnetic moment compensation behavior.

Recently Fe_2NiZ Heusler alloys, where Z = Al, Ga, Si or Ge, have also been synthesized and investigated experimentally [39]. However, to date the study of their properties through ab initio simulations has not been thorough and our aim in this paper is to fill this gap by carrying out extensive numerical computations using the LAPW method. Our objective is to explore changes in the electronic, magnetic, structural, elastic and thermoelectric properties as we gradually modify the Ga content of the alloy $Fe_{2-x}NiGa_{1+x}$ and make the transition from Fe_2NiGa to $FeNiGa_2$.

Our paper is organized as follows: Sect. 2 gives details about our computational approach while Sect. 3 presents and discusses our results. Finally, Sect. 4 concludes our paper and summarizes our main findings.

2 Computational details

The space group of X_2YZ full Heusler alloys is $Fm\bar{3}m$ [18] with a unit cell made out of four interpenetrating face centered cubic (FCC) sub-lattices *A, B, C and D* having, respectively, the following Wyckoff coordinates (0 0 0), (1/4 1/4 1/4), (1/2 1/2 1/2) and (3/4 3/4 3/4). If the X atoms have more valence electrons than the Y's, then they occupy the two equivalent crystallographic sites *A* and *C* while the Y and Z atoms occupy the *B* and *D* sites, respectively [18]. On the other hand, if the valence electron number of the X atoms is less than that of the Y atoms, the alloy crystallizes in the Hg_2CuTi-type structure with the space group $F\bar{4}3m$ [18].

The calculations we are reporting in this paper are performed using the FP-LAPW method [44] as implemented in the WIEN2K package [45]. They are based on the spin-polarized density functional theory (DFT), which has proven very reliable in the simulation of the ground state properties of materials [46, 47]. The exchange–correlation potential is treated within both the local density (LDA) and generalized gradient approximations (GGA) of Perdew as parameterized by Burke and Ernzerhof (PBE) [48].

In our calculations, the FP-LAPW basis set consists of the $3d^6 4s^2$ states of Fe, $3d^8 4s^2$ states of Ni and $4s^2 4p^1$ states of Ga. For the wave function expansion in terms of spherical harmonics inside the muffin-tin spheres, the maximum value for angular momentum is taken as $l_{\max} = 10$. Moreover, as far as convergence is concerned, the largest reciprocal lattice vector of the plane wave expansion inside the interstitial region is set by the condition $R_{MT} K_{\max} = 9$ with R_{MT} being the smallest muffin-tin sphere radius.

On the other hand, the magnitude of the largest vector in the charge density Fourier expansion was up to $G_{\max} = 12(a.u.)^{-1}$. A dense mesh of 1000 k-point is used and the tetrahedral method [49] is employed for integration over the first Brillouin zone (BZ). We consider our calculations to have converged to self-consistency only when successive values of the charge difference are less than $(10^{-3}e)$ according to the charge convergence criterion [45].

The thermoelectric properties of Fe_{2-x} $NiGa_{1+x}$ materials are calculated by applying Boltzmann's transport theory as implemented in the BoltzTraP code [50] where we use a dense *k*-mesh ($50 \times 50 \times 50$) to ensure the convergence of transport calculations.

3 Results and discussion

3.1 Structural properties

In order to simulate the following ternary alloys $Fe_{1.75}NiGa_{1.25}$, $Fe_{1.5}NiGa_{1.5}$ and $Fe_{1.25}NiGa_{1.75}$, we start with the conventional 16 atom ($1 \times 1 \times 1$) supercell, then substitute one atom of Fe by Ga in $Fe_{1.75}NiGa_{1.25}$, two atoms of Fe by Ga in $Fe_{1.5}NiGa_{1.5}$ and finally three atoms of Fe by Ga in $Fe_{1.25}NiGa_{1.75}$ as shown in Fig. 1 [51, 52].

A word on the symmetry of our systems is in order at this point. Indeed, the crystal symmetry of these alloys is *x* dependent, to be specific for $x = 0.25$ and 0.75, the alloys have the P-43 m (215) space group symmetry while for $x = 0.5$ it is the P-42 m (111) one. Going further to the extreme values $x = 0$ and $x = 1$ where the conventional cell comprises only 4 atoms, the space group symmetries become, respectively, F-43 m (216) and Fm-3 m (225) [39–42].

To calculate the ground state properties of these ternary alloys, we follow common practice: First we optimize the total energy as a function of the unit cell volume, computation of the

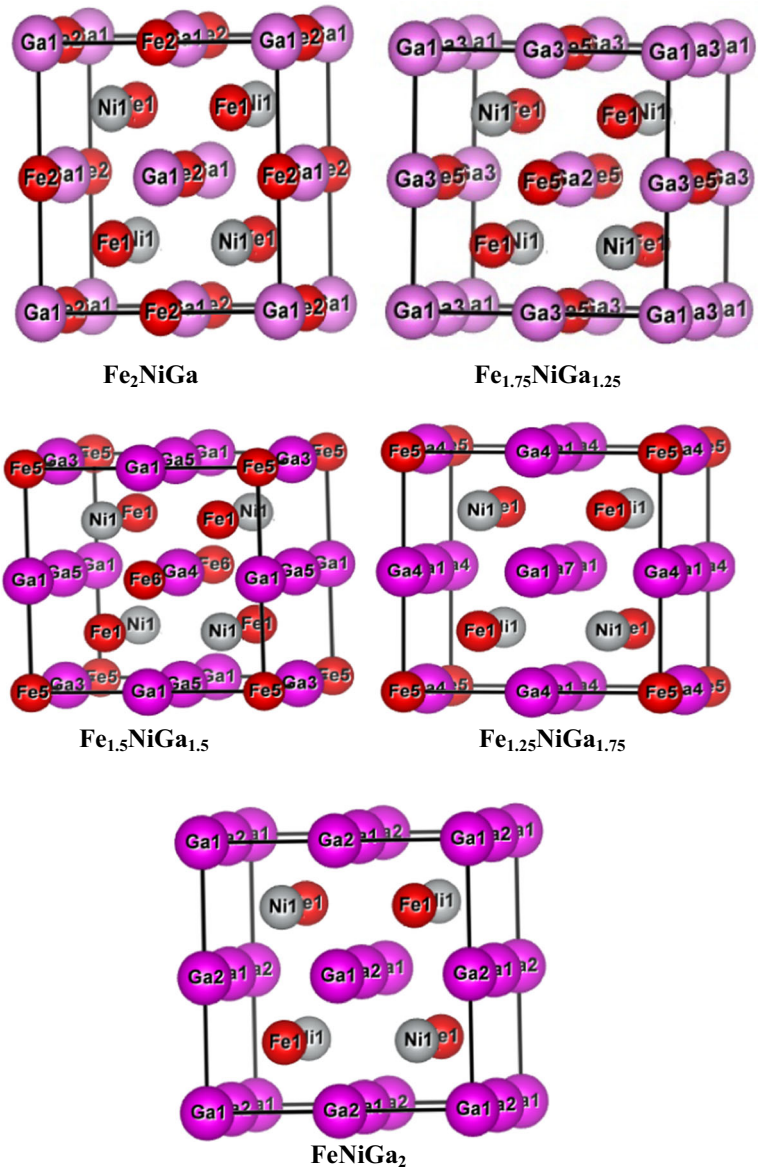

Fig. 1 Unit cell structure of the $Fe_{2-x}NiGa_{1+x}$ alloy

lattice constants, bulk modulii and first pressure derivatives of the latter then follow from Murnaghan's equation of state [53].

To determine the most stable structure among the $Fe_{2-x}NiGa_{1+x}$compounds, we relied on minimizing the total energy. In this procedure, for different cell volumes around the equilibrium one V_0, crystal total energies are calculated in both phases, Cu_2MnAl and Hg_2CuTi and compared to each other as shown on Fig. 2.

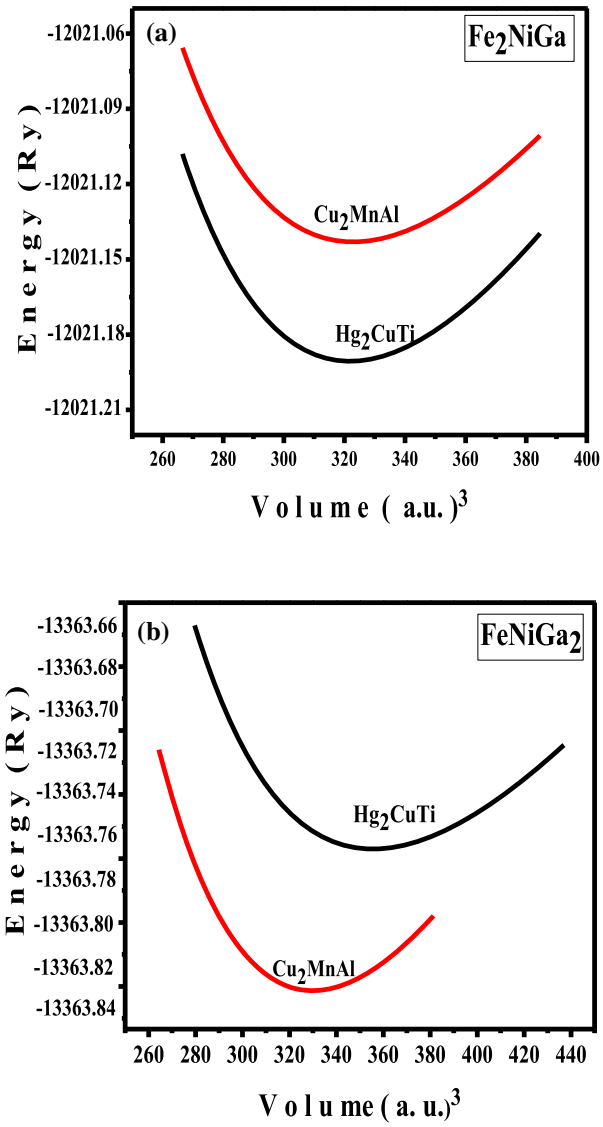

Fig. 2 Calculated total energy as a function of the unit cell volume for Fe_2NiGa and $FeNiGa_2$ in both the Cu_2MnAl and Hg_2CuTi phases

From Fig. 2a it is clear that the Hg_2CuTi-phase of Fe_2NiGa has the lower energy; therefore, this phase is the most stable at ambient pressure. For the $FeNiGa_2$ compound, see Fig. 2b, the situation reverses and this time the Cu_2MnAl phase is the more stable one. These results agree with those obtained by Zhang et al. [54] who use the pseudopotential method (Table 1).

The calculated lattice parameters a, bulk moduli B_0 and pressure derivatives of the latter for the $Fe_{2-x}NiGa_{1+x}$alloys ($x = 0.0, 0.25, 0.5, 0.75, 1$) are listed in Table 2 along with the available experimental [54] and theoretical [55] data for comparison. We note that when com-

Table 1 Calculated equilibrium lattice constants, bulk moduli B_0, pressure derivatives of the bulk moduli B' and the minimal energy for the $Fe_{2-x}NiGa_{1+x}$ ($x = 0.0, 0.25, 0.5, 0.75, 1$) alloys

X	*GGA*				*LDA*			
	a (Å)	*B*(*GPa*)	*B'*	*E*(*Ry*)	*a* (Å)	*B*(*GPa*)	*B'*	*E*(*Ry*)
0	5.7569 5.776 [54] 5.76 [55]	172.41 174.82 [55]	4.98 4.40 [55]	−12,021.190	5.599	214.71	4.64	−12,001.858
0.25	5.7713 5.82 [54]	164.02	5.58	−12,356.852	5.610	209.79	5.23	−12,337.244
0.5	5.7937 5.80 [54]	154.00	5.22	−12,692.513	5.627	213.41	5.86	−12,672.627
0.75	5.8100 5.78 [54]	146.81	5.31	−13,028.173	5.637	203.34	5.87	−13,008.010
1	5.8045 5.76 [54]	166.61	4.51	−13,363.832	5.657	206.30	5.02	−13,343.395

Table 2 Calculated total and partial magnetic moments m_s (in units of μ_B) and Curie temperatures for the $Fe_{2-x}NiGa_{1+x}$ ($x = 0.0, 0.25, 0.5, 0.75, 1$) alloys for various compositions

X	ms						T_C
	Tot	Fe(A)	Fe(B)	Ni	Ga	Interstitiel	
0	4.8623 5 [54] 4.82 [39]	1.834 2 [54]	2.62 2.7 [54]	0.4998 0.25 [54]	−0.03	−0.06	902.66 850 [54] 785 [39]
0.25	3.851 4 [54]	1.648 1.5 [54]	2.59 2.7 [54]	0.364 0.0 [54]	−0.034	−0.267	719.85 800 [54]
0.5	3.057 3 [54]	1.56 1.3 [54]	2.61 2.7 [54]	0.2858 0.0 [54]	−0.026	−0.267	576.32 700 [54]
0.75	2.036 2.0 [54]	1.285 1.0 [54]	2.617 2.7 [54]	0.2858 0.0 [54]	−0.026	−0.206	391.52 500 [54]
1	0.80 0.8 [54]	0.794 0.8 [54]	–	0.093 0.0 [54]	−0.018	−0.04	167.8 180 [54]

pared with experimental values [54], our calculated lattice parameters for the $Fe_{2-x}NiGa_{1+x}$($x = 0.0, 0.25, 0.5, 0.75, 1$) alloys show deviations of less than 1%, agreement is therefore excellent.

We show in Fig. 3 the calculated equilibrium lattice constants of the $Fe_{2-x}NiGa_{1+x}$alloys ($x = 0.0, 0.25, 0.5, 0.75, 1$) as functions of the *Ga* excess concentration *x*. We notice that as more Fe atoms are replaced by Ga atoms, the lattice constant increases, moreover a clear non-monotonous behavior of the lattice constant can easily be seen. The behavior of the lattice constant is easily understood if we recall that the atomic radius of Ga, which is 1.38 Å, is larger than that of Fe, which is 1.25 Å [56]. The anomaly for $x \geqslant 0.75$, where the lattice constant starts decreasing is attributed to the enhanced covalent binding between transition metal and main group atoms. Concerning the bulk modulus B_0, its behavior is the reverse of that of the calculated equilibrium lattice constants as shown on the same figure.

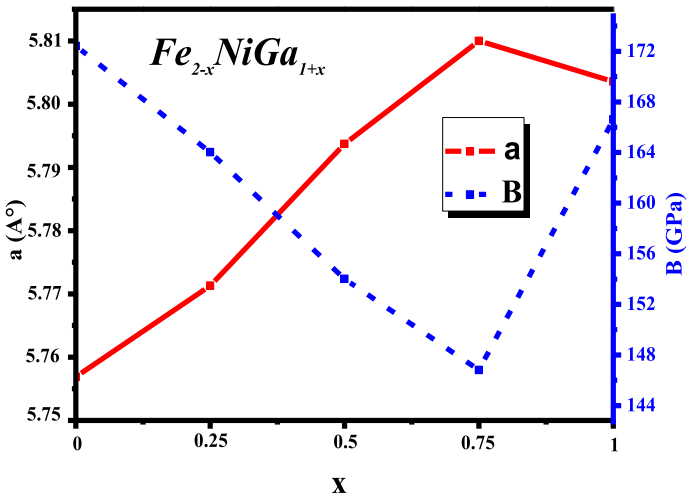

Fig. 3 Lattice constant (left axis) and bulk modulus (right axis) of the $Fe_{2\text{-}x}NiGa_{1+x}$ alloy as a function of Ga excess x

3.2 Electronic properties

We begin our discussion of the electronic structure with the density of states (DOS), both total and projected, which we computed within the GGA for both spin orientations. Our results, shown on Fig. 4, agree well with those of Zhang et al. [54] who studied the total electronic density of states (DOS) and the partial (DOS) of p and d electrons for both Fe_2NiGa and $FeNiGa_2$.

It can clearly be seen that the substitution of Fe by Ga in $Fe_{2-x}NiGa_{1+x}$ does not change completely the overall shape of the total DOS. For the majority spin, the DOS is basically below the Fermi energy E_F, while in the case of the minority spin, the anti-bonding peak is shifted high above E_F due to the exchange splitting [57]. While the p-states of the Z elements hybridize with the d-states of Fe and Ni, the total bands are formed mostly of the d-states of Fe and Ni.

A close look at our numerical results shows that for energies in the range −3.2 to 1.5 eV the main contribution to the DOS comes chiefly from the 3d states of Fe and Ni. Moreover, the DOS is widely spread due to the strong d-d hybridization as Fig. 4 clearly shows. In addition, we note that the total DOS exhibits peaks both below and above the Fermi energy E_F which are due to coupling between the bonding and anti-bonding states between Fe and Ni atoms.

For the d states DOS of Ni (B), the bonding and anti-bonding peaks are below the Fermi level for both spin orientations. As a result, the exchange splitting of Ni (B) is weaker when compared to those of Fe (A) and Fe (B), thus giving rise to a small spin magnetic moment on the Ni (B) site.

In Fig. 5a,b for the spin-down case we also observe around −3.2 eV below E_F an overlap of the peaks of the p and d states which is a clear signature of p–d hybridization. Due to the exchange-splitting arising from the Weiss molecular field, while the minority spin states shift toward E_F the majority spin states shift toward more negative energies, which goes in the way of favoring ferromagnetism for our alloys.

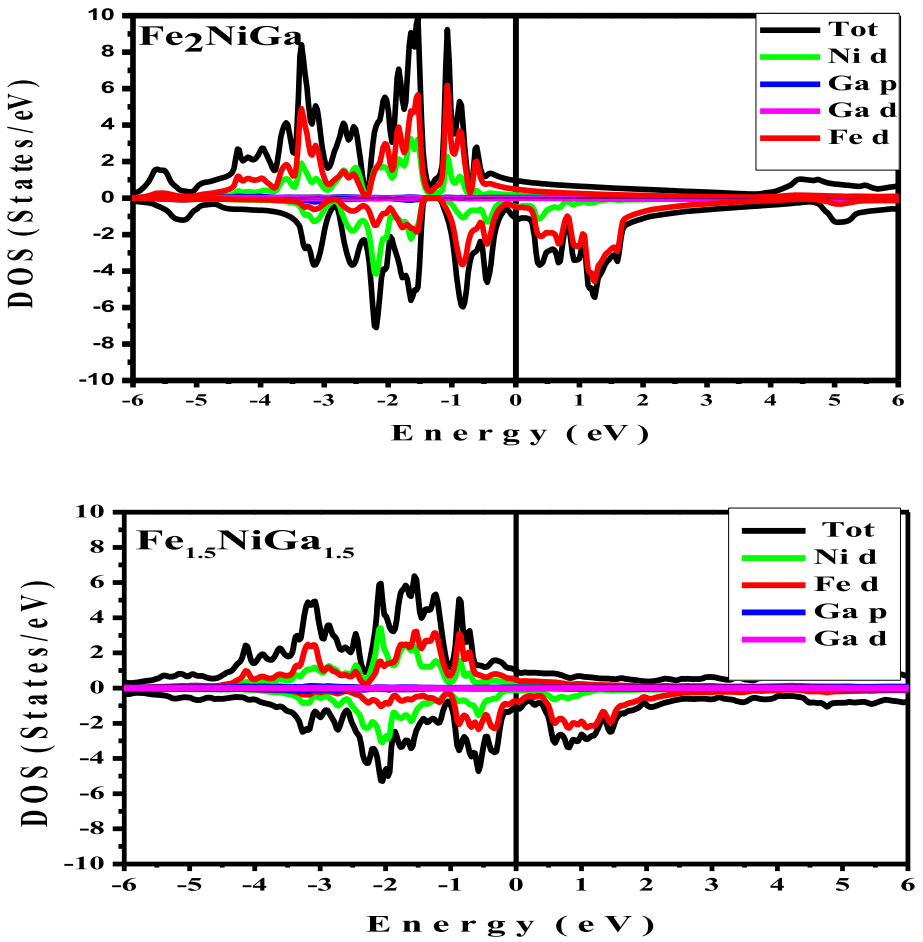

Fig. 4 Calculated density of states (total DOS and PDOS) for Fe_2NiGa and $Fe_{1.5}NiGa_{1.5}$

In Fig. 5c, we show the total DOS of the $Fe_{2-x}NiGa_{1+x}$ ($x = 0.0, 0.25, 0.5, 0.75, 1$) alloys, we very clearly see the gradual disappearance of the exchange spin splitting as we go from Fe_2NiGa to $FeNiGa_2$.

Using our theoretical equilibrium lattice constant, for the ternary Heusler alloys Fe_2NiGa and $Fe_{1.5}NiGa_{1.5}$, we have calculated the band structure along the high symmetry directions of the first Brillouin zone and our results are depicted on Fig. 6 where the Fermi levels in both cases are set to 0 eV.

As we go from Fe_2NiGa to $FeNiGa_2$, we note that the spin-down states in all alloys are shifted to higher energies above Fermi level. We attribute this shifting of bands to the spin polarization responsible of the exchange interaction. We note in passing that the lack of a gap at the Fermi level, for all compounds and for both spin channels as clearly seen in Fig. 6 points to the metallic character of these materials.

We have also computed the electronic charge densities in the (110) plane in order to investigate the bonding character between the atoms in our systems and our results are

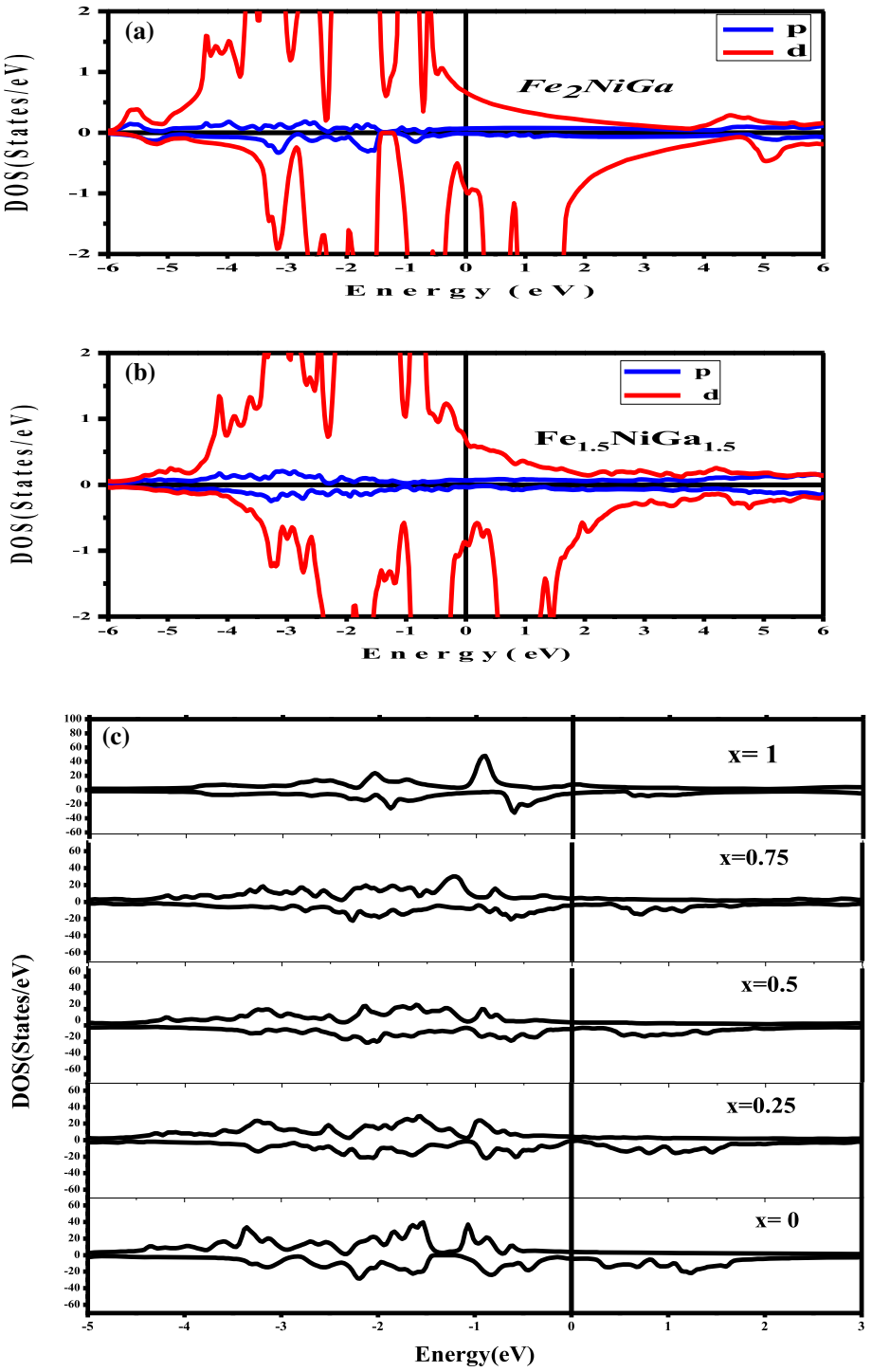

Fig. 5 Partial DOS for p and d states of Fe_2NiGa and $Fe_{1.5}NiGa_{1.5}$ **(a–b)** and total DOS for $Fe_{2-x}NiGa_{1+x}$ **(c)**

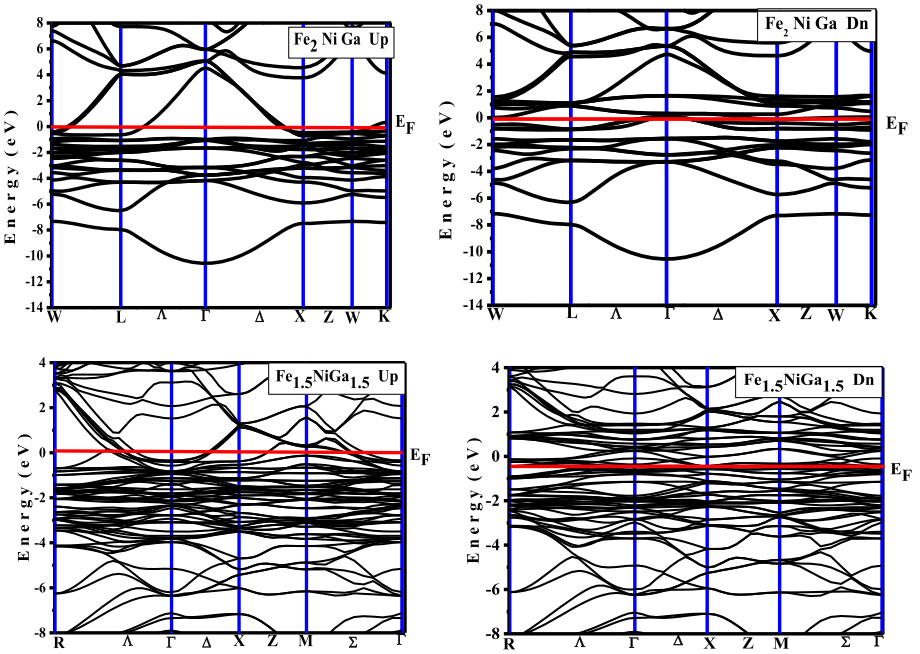

Fig. 6 Spin up and down band structures of $Fe_{2-x}NiGa_{1+x}$ alloys for $x = 0$ and $x = 0.5$

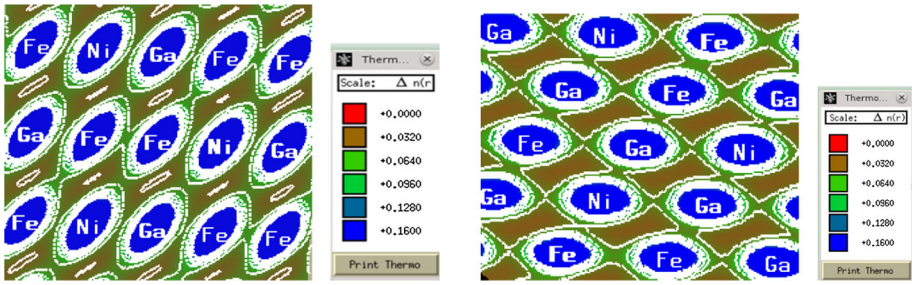

Fig. 7 Calculated electronic charge densities for Fe_2NiGa and $Fe_{1.5}NiGa_{1.5}$ in the (110) plane

displayed in Fig. 7. It can be seen quite easily that our alloys exhibit different electron distributions depending on x, the excess *Ga* concentration in the alloys.

Let us concentrate on the close neighbors of the Ni atom in the Fe_2NiGa compound: We clearly see covalent bonds between this Ni atom and the two atoms Fe and Ga. On the other hand, just lone pairs appear between the Ni atom and the other Fe atom.

As we make the transition from Fe_2NiGa to $FeNiGa_2$, the neighborhood of Ni changes, and the covalent bonding gets more and more dominant until it manifest itself fully at the extreme end. This confirms the competition between the *p–d* and *d–d* orbital hybridizations whereby the former increases at the expense of the latter.

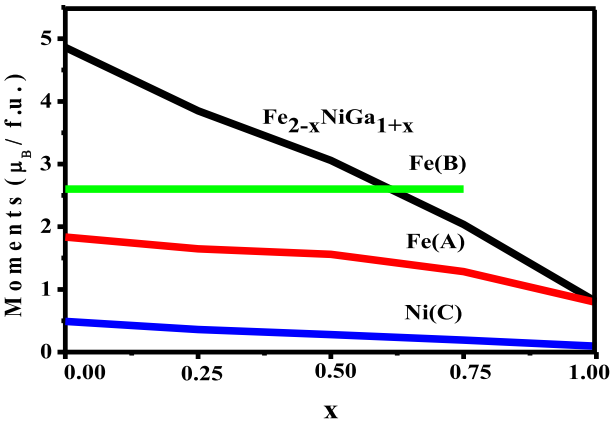

Fig. 8 Total and local spin magnetic moments of $Fe_{2-x}NiGa_{1+x}$ alloys for various compositions

3.3 Magnetic properties

We have also explored the magnetic properties of our systems, the corresponding results are summarized in Table 2 where we see that our calculated total and partial magnetic moments and Curie temperatures for the $Fe_{2-x}NiGa_{1+x}$ alloys are in good agreement with previous theoretical and experimental data reported by other authors [39, 54, 55].

In units of the Bohr magneton μ_B, the calculated values of the total magnetic moments are as follows: 4.86 for Fe_2NiGa, 3.85 for $Fe_{1.75}NiGa_{1.25}$, 3.057 for $Fe_{1.5}NiGa_{1.5}$, 2.036 for $Fe_{1.25}NiGa_{1.75}$ and 0.79 for $FeNiGa_2$. The calculated moments of $Fe_{2-x}NiGa_{1+x}$ alloys show a linear decrease with increasing *Ga* content. Likewise, the partial moments of Fe (A) and Ni (C) also decrease linearly contrary to that of the Fe (B) which remains almost constant as Fig. 8 shows**.**

Our computations clearly show that Fe (A) and Fe (B) have different atomic magnetic moments thus indicating the influence of the atomic environment. Moreover, we find that the atomic magnetic moment of Ni (C) is small and parallel to that of Fe (A) and Fe (B) atoms. On the other hand, that of Ga in addition to being small is found to be anti-parallel. For all Ga excess concentrations x, our calculations therefore hint that the $Fe_{2-x}NiGa_{1+x}$ ($x = 0.0$, 0.25, 0.5, 0.75, 1) alloys should all be ferromagnetic.

From Table 2, we clearly see that the cell total magnetic moment draws its main contributions from the Fe (A) and Fe (B) atoms. In the present alloys, the atomic moments of the Fe atoms at the A site range from 1.83 to $0.79\mu_B$, at the B site on the other hand a roughly constant value of $2.6\mu_B$ is obtained throughout.

When we change the concentration of Fe atoms as we go from Fe_2NiGa to $FeNiGa_2$, we note that the atoms surrounding Fe (B) are always the same: Four Fe (A) atoms and four Ga atoms. On the other hand, the atoms surrounding Fe(A) change as a result of substituting Fe atoms by Ga ones, this process dilutes the concentration of magnetic atoms and changes the neighboring relationship of Fe–Fe or Fe–Ni from nearest neighbors to next-nearest neighbors. This further weakens the *d–d* exchange interaction between Fe and Ni, this is the reason behind the near constancy of the magnetic moment of Fe (B) and the decreasing trend of that of Fe (A).

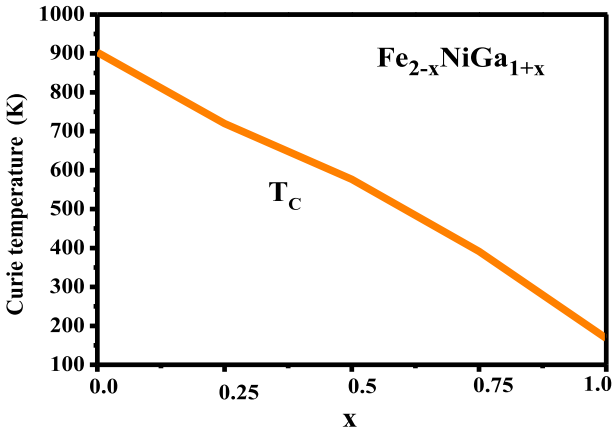

Fig. 9 Curie temperature of the $Fe_{2-x}NiGa_{1+x}$ alloy as a function of x

At this point, we should point out that our results do not follow the Slater–Pauling rule whereby the unit cell magnetic moment $M = Z\text{-}24$, where Z is the number of valence electrons in the unit cell as was found for instance in Co_2FeAl and Co_2FeSi [58, 59].

It should also be noted that our calculated values m_{tot} for the total magnetic moments are not integers, as it is typical for half-metallic ferromagnets with a band gap for the minority states at E_F [58, 59].

Using the model of Ref. [59], we have also made estimations of the respective Curie temperatures T_C for the $Fe_{2-x}NiGa_{1+x}$ alloys using the relation $T_C = 23 + 181\ m_{tot}$. Our calculated values for T_C are presented in Table 2 along other data. The values found are as follows: 902.66 K, 719.85 K, 576.32 K, 391.52 K and 167.8 K for Fe_2NiGa, $Fe_{1.75}NiGa_{1.25}$, $Fe_{1.5}NiGa_{1.5}$, $Fe_{1.25}NiGa_{1.75}$ and $FeNiGa_2$, respectively. As expected, T_C decreases with increasing Ga content in the $Fe_{2-x}NiGa_{1+x}$ alloys, moreover this decrease is linear as shown in Fig. 9. So, the substitution of Fe by Ga weakens the ferromagnetic interaction and decreases T_C. Additionally, it is worth mentioning that the magnetic moments in Heusler alloys are weakened by covalent bonding as it has been reported in [60, 61]. This means that in the case of strong covalent bonding, a system should have a lower T_C. This is consistent with our results and could reasonably be invoked to explain the decrease of T_C as more Ga atoms substitute Fe.

3.4 Elastic properties

Solids with cubic symmetry are characterized by only three independent elastic constants namely C_{11}, C_{12} and C_{44}. Elastic stability imposes the following conditions known as the Born–Huang criteria [62, 63] which read as follows

$$\begin{aligned} &C_{11}\rangle 0, C_{12}\rangle 0 \\ &C_{11} - C_{12}\rangle 0, C_{11} + 2C_{12}\rangle 0 \end{aligned} \tag{1}$$

The calculated constants C_{ij} allow us to obtain other widely used macroscopic elastic parameters for our alloys, in particular the bulk and shear modulii B and G, respectively.

We should mention here that Hill [64, 65] has shown that the upper and lower limits of the actual effective modulus are given respectively by the Voigt and Reuss modulii. It follows

Table 3 Elastic constants C_{11}, C_{12} and C_{44} and bulk modulus B(in GPa) for Fe_{2-x} $NiGa_{1+x}$ (x = 0.0, 0.25, 0.5,0.75,1) using GGA

Alloys	C_{11}	C_{12}	C_{44}	B
Fe_2NiGa	209.61 248.31 [55]	157.239 139.14 [55]	125.404 119.27 [55]	174.696 175.53 [55]
$Fe_{1.75}NiGa_{1.25}$	201.83	150.63	119.167	167.698
$Fe_{1.5}NiGa_{1.5}$	188.99	136.467	104.23	153.97
$Fe_{1.25}NiGa_{1.75}$	188.11	134.36	102.94	152.27
$FeNiGa_2$	182.53	130.035	107.70	147.53

then that the arithmetic average of the Voigt and Reuss modulii yields the Voigt–Reuss–Hill modulus [66, 67].

For a cubic structure the expressions for the Voigt, Reuss and Voigt–Reuss–Hill shear modulii respectively denoted by G_v G_R, and G_H [64, 65, 67] as well as the bulk modulus B, Poisson's ratio σ, Young's modulus E and elastic anisotropic factor A are given by the following:

$$\begin{aligned} G_V &= (C_{11} - C_{12} + 3C_{44})/5 \\ G_R &= 5(C_{11} - C_{12})C_{44}/(4C_{44} + 3(C_{11} - C_{12})) \\ G_H &= (G_V + G_R)/2 \\ B &= B_V = B_R = (C_{11} + 2C_{12})/3 \\ \sigma &= (3B - 2G)/2(3B + G) \\ E &= 9BG_H/3B + G_H \\ A &= 2C_{44}/(C_{11} - C_{12}) \end{aligned} \tag{2}$$

The three independent elastic constants C_{11}, C_{12} and C_{44} are obtained directly from first principles calculations while the remaining quantities G_V, G_R, G_H,B, σ, E and A are readily deduced from these.

The Debye temperature is estimated from the average sound velocity v_m [68]! from

$$\theta_D = \frac{h}{k_B}\left(\frac{3n}{4\pi V_a}\right)^{\frac{-1}{3}} v_m, \tag{3}$$

where h and k_B are, respectively, Planck's and Boltzmann's constants while n is the number of atoms per unit cell and V_a its volume.

We notice from Table 3 that our calculated elastic constants [C_{11}, C_{12} and C_{44} for all five alloys satisfy the Born stability criteria alluded to previously in the text. We can also see that the values of the bulk modulus B deduced from the elastic constants C_{ij}, given in Table 3, agree well with those calculated from the equation of states (EOS) given in Table 1. This agreement in cross-checking speaks in favor of our calculated elastic constants C_{ij}.

The difference $C_{11} - C_{44}$ known as Cauchy's pressure is an indicator of the material's ductility [69]. Ductile materials are characterized by a positive Cauchy pressure while the opposite is true, i.e., brittle materials have a negative Cauchy pressure. According to this criterion, all our alloys should be ductile since our calculated Cauchy pressures are all positive.

Resistance to compression and plastic deformations are related, respectively, to the bulk and shear modulii B and G. Pugh's B/G criterion was proposed [70] as an empirical malleabil-

ity measure for polycrystalline materials. If *B/G is* greater than 1.75, the material is expected to be ductile, on the other hand if *B/G* is less than 1.75, the material will show brittleness instead. In our case, the *B/G* ratio (see Table 4) is greater than 1.75 for all alloys. Therefore, conclusions from Pugh's index of ductility agree perfectly with the Cauchy pressure criterion in the present situation.

We now turn to a discussion of the Poisson ratio σ which can give important information on the nature of the atomic bonding in the sample. Typical values for σ are 0.1 for covalent materials, 0.25 for ionic compounds and 0.33 for metallic materials [70]. In our case $\sigma =$ 0.33, a significant metallic contribution to the inter-atomic bonds for these alloys should be expected.

In addition, for covalent, ionic and metallic materials, typical relations between the bulk and shear modulii are $G \sim 1.1B$, $G \sim 0.6B$ and $G \sim 0.4B$, respectively [71]. In our case, the calculated value of G/B is ~ 0.39, which in accordance with the calculated values of Poisson's ratio just discussed (see Table 4), indicates that our alloys should be metallic.

Another important parameter is the elastic anisotropic factor A, which is a measure of the degree of elastic anisotropy in the solid. For crystals with isotropic elastic properties, A is unity and deviation from this value measures the amount of elastic anisotropy. The calculated value of the anisotropy factor for our alloys is greater than 1, which means that these alloys are anisotropic when it comes to their elastic properties.

In elasticity theory, Young's modulus E defined as the ratio of the tensile stress to the corresponding tensile strain provides information about stiffness, materials with higher values of E are considered stiffer than those with lower E values. Hence, based on the present study, we can infer that the stiffness of Fe_{2-x} $NiGa_{1+x}$ (x = 0.0, 0.25, 0.5, 0.75, 1) follows the following order Fe_2 NiGa > $Fe_{1.75}$ $NiGa_{1.25}$ > FeNiGa_2 > $Fe_{1.5}$ $NiGa_{1.5}$ ~ $Fe_{1.25}$ $NiGa_{1.75}$. We note that the theoretical results of Ref. [55] do not agree well with ours and we attribute the difference between both results to the different methods adopted in each work. In the absence of available experimental data in the literature, we consider the present results as predictive and future experimental work is much needed.

3.5 Transport properties

The thermoelectric properties of the Fe_{2-x} $NiGa_{1+x}$ alloys are obtained using the BoltzTraP code [50]. The latter has proven very effective in calculating the electronic transport properties [72], namely the electrical conductivity σ, the Seebeck coefficient S, the thermal conductivity κ and the figure of merit (ZT). For theoretical exposition of thermoelectric properties, we refer the reader to refs. [73, 76].

Our calculated Seebeck coefficient for Fe_{2-x} $NiGa_{1+x}$ are plotted against the chemical potential in Fig. 10. The computed values of S for Fe_{2-x} $NiGa_{1+x}$ are negative indicating the n-type character of the charge carrier in the Fe_{2-x} $NiGa_{1+x}$ compound. As the temperature increases, S decreases.

Thermal conductivity is the ability of a material to conduct heat, it is due to charge carriers and lattice vibrations. While in metals free electrons are responsible for both electrical and thermal conduction, in semi-metals and semiconductors heat transfer is assured by both electrons and holes [76]. We have calculated the electronic thermal conductivity of our alloys, the results are shown in Fig. 11. Note that the thermal conductivity is an increasing function of temperature in both alloys for positive chemical potentials, the maxima reached at 900 K being in units of W/mKs 26.74, 15.66, 15.84, 12.16 and 13.56 respectively for Fe_2 NiGa, $Fe_{1.75}$ $NiGa_{1.25}$, $Fe_{1.5}$ $NiGa_{1.5}$, $Fe_{1.25}$ $NiGa_{1.75}$ and FeNiGa_2.

Table 4 Voigt–Reuss–Hill shear modulus G_H, Poisson's ratio σ, Young's modulus E, elastic anisotropic factor A, Cauchy's pressure, Pugh's index and Debye temperature for Fe_{2-x} $NiGa_{1+x}$ (x = 0.0, 0.25, 0.5,0.75,1) using GGA

Alloys	G_H	σ	E	A	C_{12}-C_{44}	B/G_H	θ_D
Fe_2NiGa	67.78 93.39 [55]	0.328 0.27 [55]	180.06 237.97 [55]	4.78 2.18 [55]	31.84 19.88 [55]	2.57 1.88 [55]	416.014 385.17 [55]
$Fe_{1.75}NiGa_{1.25}$	65.07	0.328	172.85	4.65	31.46	2.57	405.196
$Fe_{1.5}NiGa_{1.5}$	60.34	0.326	160.112	3.97	32.24	2.55	388.335
$Fe_{1.25}NiGa_{1.75}$	60.39	0.324	160.035	3.83	31.42	2.52	386.051
$FeNiGa_2$	61.58	0.316	162.19	4.10	22.33	2.39	386.568

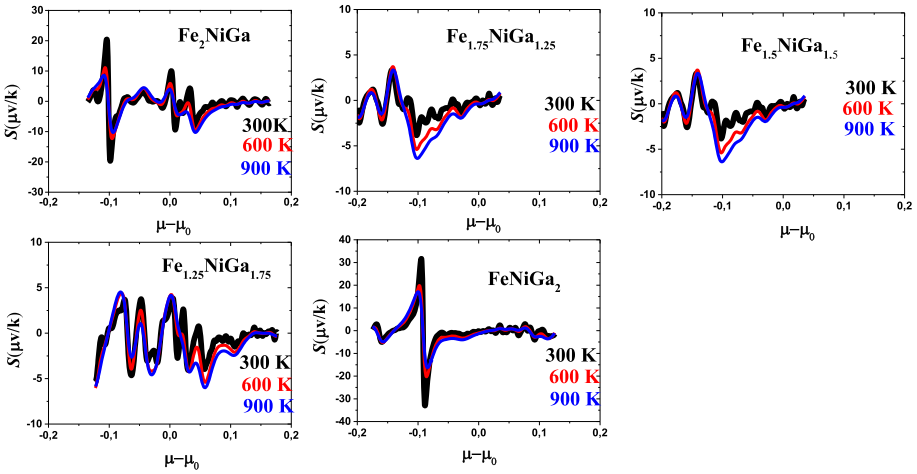

Fig. 10 Seebeck coefficient of $Fe_{2-x}NiGa_{1+x}$

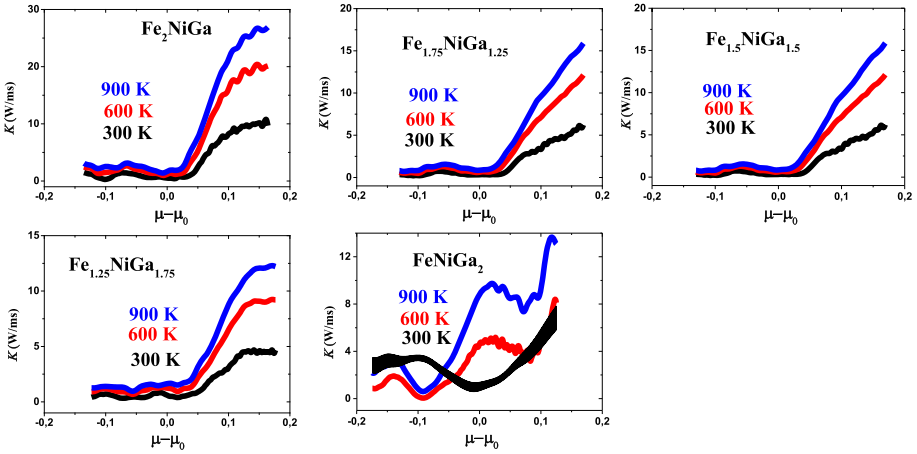

Fig. 11 Thermal conductivity of $Fe_{2-x}NiGa_{1+x}$

Our calculated electrical conductivity σ is shown in Fig. 12 at different temperatures as a function of the chemical potential. Our results show that the electrical conductivity overall behavior does not change much as T changes from 300 to 900 K.

Our calculated *ZT* for Fe_{2-x} $NiGa_{1+x}$ is plotted in the Fig. 13 which clearly shows that this parameter exhibits oscillations as a function the chemical potential and is quite sensitive to temperature. Comparing the different panels of this figure among themselves, we infer that the figure of merit ZT is strongly material dependent. The lack of published work on the thermoelectric properties of these alloys does not allow for a comparison, so our results should be taken a reference for future work either theoretical or experimental.

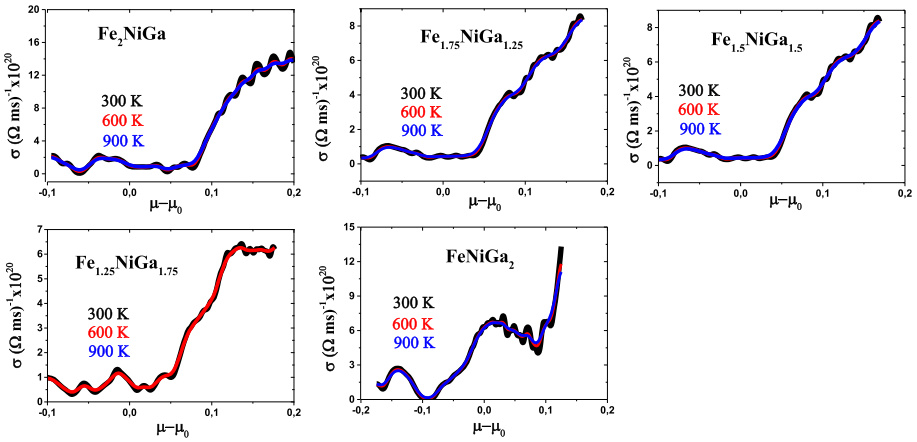

Fig. 12 Electrical conductivity of $Fe_{2-x}NiGa_{1+x}$

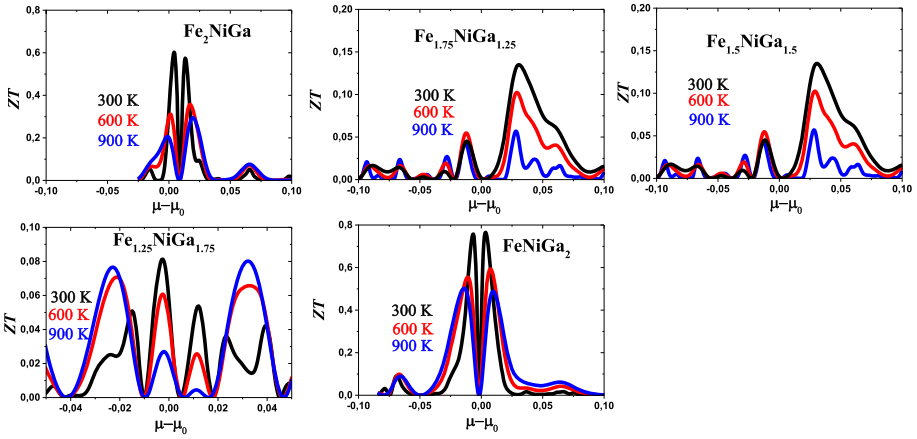

Fig. 13 Thermoelectric figure of merit (ZT) of $Fe_{2-x}NiGa_{1+x}$

4 Conclusion

The study conducted in the present paper investigated the structural, electronic, magnetic and elastic properties of the $Fe_{2-x}NiGa_{1+x}$ Heusler alloys for the following values of x: 0, 0.25, 0.5, 0.75, 1. In our work, we used the full-potential linearized augmented plane waves (FP-LAPW) method as implemented in the *WIEN2k* code to find out the extent to which the *Ga* excess concentration x affects key physical properties of these compounds.

We computed the equilibrium lattice constants for the $Fe_{2-x}NiGa_{1+x}$ Heusler alloys ($x =$ 0, 0.25, 0.5, 0.75, 1) and found excellent agreement with available experimental data.

The lack of a gap at the Fermi level signals the metallic character for the $Fe_{2-x}NiGa_{1+x}$Heusler alloys for the following x values 0, 0.25, 0.5, 0.75, 1. Moreover, the substitution of Fe by Ga dilutes further the concentration of magnetic atoms and changes the neighboring relationship of Fe–Fe or Fe–Ni from nearest neighbors to next-nearest neighbors. This further weakens the d–d exchange interaction between Fe and Ni and results in a decrease of the unit cell total magnetic moment and a concomitant lowering of the Curie

temperature. Moreover, by monitoring the concentrations of Fe and Ga, we have been able to modify the magnetic properties.

From our calculated elastic constants and the application of the criteria for mechanical stability, we infer that $Fe_{2-x}NiGa_{1+x}$ ($x = 0, 0.25, 0.5, 0.75, 1$) should be stable at ambient pressure, in addition, the values of their B/G ratio should make them ductile.

The thermoelectric properties of these compounds are investigated through the calculation using the Boltztrap code of key quantities such as the thermal and electrical conductivities as well as the Seebeck coefficient.

Acknowledgements S. Lamari is grateful to the Ministry of Higher Education for a research grant through CNEPRU research project NBR B00L02UN190120150003 and S. Chami thanks Dr. H. Baaziz for technical help while installing Wien2k.

References

1. X. Guo-Liang, C. Jing-Dong, C. Dong, M. Jiang-Zhong, Y. Ben-Hai, S. De-Heng, Chin. Phys. B **18**, 744 (2009)
2. V.A. Chernenko, A. Fujita, S. Bessighini, J.I. Pérez-Landazabal, J. Magn. Magn. Mater **320**, e156–e159 (2008)
3. E. Shreder, S.V. Streltsov, A. Svyazhin, A. Makhnev, V.V. Marchenkov, A. Lukoyanov, H.W. Weber, J. Phys. Condens. Matter **20**, 045212 (2008)
4. S. Sanvito, C. Oses, J. Xue, A. Tiwari, M. Zic, T. Archer, P. Tozman, M. Venkatesan, M. Coey, S. Curtarolo, Sci. Adv. **3**, e1602241 (2017)
5. Y.K. Takahashi, A. Srinivasan, B. Varaprasad, A. Rajanikanth, N. Hase, T.M. Nakatani, S. Kasai, T. Furubayashi, K. Hono, Appl. Phys. Lett. **98**, 152501 (2011)
6. L. Galdun, V. Vega, Z. Vargová, E.D. Brriga-Castro, C. Luna, R. Varga, V.M. Prida, Appl. Nano Mater. **1**, 7066–7074 (2018)
7. Z. Wen, T. Kubota, K. Takanashi, J. Phys. D Appl. Phys. **51**, 435002 (2018)
8. Z. Wen, T. Kubota, T. Yamamoto, K. Takanashi, Sci. Rep. **5**, 18387 (2015)
9. M. Enamullah, S.-C. Lee, J. Alloys Compd. **765**, 1055–1060 (2018)
10. A. Dehghan, S. Davatolhagh, J. Alloys Compd. **772**, 132–139 (2019)
11. L. Chen, Y. Liu, J. He, T.M. Tritt, S.J. Poon, AIP Adv. **7**, 0652208 (2017)
12. M. Gürth, G. Rogl, V.V. Romaka, A. Grytsiv, E. Bauer, P. Rogl, Acta Mater. **104**, 210–222 (2016)
13. R. He, H. Zhu, J. Sun, J. Mao, H. Reith, S. Chen, G. Schierning, K. Nielsch, Z. Ren, Mater. Today Phys. **1**, 24–30 (2017)
14. B. Ramachandran, Y.H. Lin, Y.K. Kuo, C.N. Kuo, A.A. Gippius, C.S. Lue, Intermetallics **92**, 36–41 (2018)
15. M.K. Yadav, B. Sanyal, J. Alloys Compd. **622**, 388–393 (2015)
16. R. Vikram, J. Kangsabanik, M. Enamullah, A. Alam, J. Mater. Chem. A **5**, 6131–6139 (2017)
17. K. Hayashi, M. Eguchi, Y. Miyazaki, J. Electron. Mater. **46**, 2710–2716 (2016)
18. T. Graf, F. Casper, J. Winterlik, B. Balke, G.H. Fecher, C. Felse, Z. Anorg, Allg. Chem. **635**, 976–981 (2009)
19. S. Wurmehl, G.H. Fecher, K. Kroth, F. Kronast, H.A. Dürr, Y. Takeda, Y. Saitoh, K. Kobayashi, H.-J. Lin, G. Schönhense, C. Felser, J. Phys. D Appl. Phys. **39**, 803 (2006)
20. T. Graf, C. Felser, S.S.P. Parkin, Prog. Solid State Ch. **39**, 1–50 (2011)
21. T. Graf, J. Winterlik, L. Müchler, G.H. Fecher, C. Felser, S.S.P. Parkin, Handbook Mag. Mater. **21**, 1 (2013)
22. S. Wurmehl and M. Wojcik, in Heusler Alloys , Properties , Growth, Applications Edited by C. Felser and A. Hirohota, Springer, New York (2016).
23. V.V. Khovailo, T. Takagi, A.N. Vasilev, H. Miki, M. Matsumoto, R. Kainuma, Phys. Stat. Sol. A **183**, R1–R3 (2001)
24. K. Ishikawa, R. Kainuma, I. Ohnuma, K. Aoki, K. Ishida, Acta Mater. **50**, 2233–2243 (2002)
25. J. Jung, G. Ghosh, G.B. Olson, Acta Mater. **51**, 6341–6357 (2003)
26. T. Miyamoto, W. Ito, R.Y. Umetsu, R. Kainuma, T. Kanomata, K. Ishida, Scr. Mater. **62**, 151–154 (2010)
27. P.J. Webster, J. Phys. Chem. Solids **32**, 1221 (1971)
28. K.H.J. Buschow, P.G. van Engen, J. Magn. Magn. Mater. **25**, 90 (1981)

29. W. Zhu, E.-K. Liu, C.-Z. Zhang, Y.-B. Qin, H.-Z. Luo, W.-H. Wang, Z.-W. Du, J.-Q. Li, G.-H. Wu, Acta Phys. Sin. **61**, 027502 (2011)
30. T. Omori, K. Watanabe, R.Y. Umetsu, R. Kainuma, K. Ishida, Appl. Phys. Lett. **95**, 082508 (2009)
31. W. Zhu, E.K. Liu, L. Feng, X.D. Tang, J.L. Chen, G.H. Wu, H.Y. Liu, F.B. Meng, H.Z. Luo, Appl. Phys. Lett. **95**, 222512 (2009)
32. M. Guezlane, H. Baaziz, F. El Haj Hassan, Z. Charifi, Y. Djaballah, J. Magn. Magn. Mater. **414**, 219–226 (2016)
33. Z. Bai, L. Shen, G. Han, Y.P. Feng, SPIN **2**, 1230006–1230021 (2012)
34. W. Wang, H. Sukegawa, K. Inomata, Appl. Phys. Exp. **3**, 93002–93004 (2010)
35. M. Yamamoto, T. Marukame, T. Ishikawa, K. Matsuda, T. Uemura, M. Arita, J. Phys. D Appl. Phys. **39**, 824–833 (2006)
36. V. Alijani, J. Winterlik, G.H. Fecher, S.S. Naghavi, C. Felser, Phys. Rev. B **83**, 184428 (2011)
37. K. Inomata, N. Ikeda, N. Tezuka, R. Goto, S. Sugimoto, M. Wojcik, E. Jedryka, Sci. Technol. Adv. Mater. **9**, 014101 (2008)
38. T. Graf, S.S.P. Parkin, C. Felser, IEEE Trans. Magn. **47**, 367 (2011)
39. Y.J. Zhang, W.H. Wang, H.G. Zhang, E.K. Liu, R.S. Ma, G.H. Wu, Phys. B Condens. Matter **420**, 86–89 (2013)
40. S.R. Barman, A. Chakrabarti, S. Singh, S. Banik, S. Bhardwaj, P.L. Paulose, B.A. Chalke, A.K. Panda, A. Mitra, A.M. Awasthi, Phys. Rev. B **78**, 134406 (2008)
41. G.J. Li, E.K. Liu, Y.J. Zhang, Y. Du, H.W. Zhang, W.H. Wang, G.H. Wu, J. Appl. Phys. **113**, 103903 (2013)
42. J. Chen, E. Liu, X. Qi, H. Luo, W. Wang, H. Zhang, S. Wang, J. Cai, G. Wu, Comput. Mater. Sci. **89**, 130 (2014)
43. G.J. Li, E.K. Liu, H.G. Zhang, J.F. Qian, H.W. Zhang, J.L. Chen, W.H. Wang, G.H. Wu, Appl. Phys. Lett. **101**, 102402 (2012)
44. D. Singh, Planes Waves, Pseudo-Potentials and the LAPW Method, Kluwer Academic Publishers, Boston, Dortrecht, London (1994).
45. P. Blaha, K. Schwarz, G.K.H. Madsen, D. Kvasnicka and J. Luitz, WIEN2k, An Augmented Plane Wave + Local Orbitals Program for Calculating Crystal Properties (Karlheinz Schwarz, Techn. Universität Wien, Austria), 2001
46. K.M. Wong, S.M. Alay-e-Abbas, A. Shaukat, Y. Fang, Y. Lei, J. Appl. Phys. **113**, 014304 (2013)
47. K.M. Wong, S.M. Alay-e-Abbas, Y. Fang, A. Shaukat, Y. Lei, J. Appl. Phys. **114**, 034901 (2013)
48. J. Perdew, K. Burke, M. Ernzerhof, Phys. Rev. Lett. **77**, 3865 (1996)
49. H.J. Monkhorst, J.D. Pack, Phys. Rev. B **13**, 5188 (1976)
50. G.K. Madsen, D.J. Singh, BoltzTraP: A code for calculating band-structure dependent quantities. Comput. Phys. Commun. **175**, 67 (2006)
51. S. Amari, R. Mebsout, S. Méçabih, B. Abbar, B. Bouhafs, Intermetallics **37**, 27 (2013)
52. H. Al-Yamani, B. Hamad, J. Electron Mater. **45**, 1101 (2016)
53. F.D. Murnaghan, Proc. Natl. Acad. Sci. USA **30**, 244 (1944)
54. Y.J. Zhang, X.K. Xi, F.B. Meng, W.H. Wang, E.K. Liu, J.L. Chen, G.H. Wu, Physica B **462**, 93 (2015)
55. D.C. Gupta, I.H. Bhat, Mater. Chem. Phys. **146**, 303 (2014)
56. I. Galanakis, K. Özdoğan, E. Şaşıoğlu, B. Aktaş, Phys. Rev. B **75**, 092407 (2007)
57. B.R.K. Nanda, I. Dasgupta, J. Phys. Condens. Matter **15**, 7307 (2003)
58. I. Galanakis, P.H. Dederichs, N. Papanikolaou, Phys. Rev. B **66**, 174429 (2002)
59. S. Wurmehl, G.H. Fecher, H.C. Kandpal, V. Ksenofontov, C. Felser, H.-J. Lin, J. Morais, Phys. Rev. B **72**, 184434 (2005)
60. T.J. Burch, J.I. Budnick, V.A. Niculescu, K. Raj, T. Litrenta, Phys. Rev. B **24**, 3866 (1981)
61. S.J. Pickart, R. Nathans, Phys. Rev. **123**, 1163 (1961)
62. J.F. Nye, *Physical Properties of Crystals* (Oxford University Press, Oxford, 1985)
63. Z.-J. Wu, E.-J. Zhao, H.-P. Xiang, X.-F. Hao, X.-J. Liu, J. Meng, Phys. Rev. B **76**, 054115 (2007)
64. R. Hill, Proc. Phys. Soc. A **65**, 349 (1952)
65. R. Hill, J. Mech. Phys. Solids **11**, 357 (1963)
66. A. Reuss, Z. Angew, Math. Mech. **9**, 49 (1929)
67. W. Voigt, *Lehrbuch Der Kristallphysik* (Teubner, Leipzig, 1928)
68. O.L. Anderson, J. Phys. Chem. Solids **24**, 909 (1963)
69. D.G. Pettifor, Mater. Sci. Technol. **8**, 345 (1992)
70. S.F. Pugh, Philos. Mag. **45**, 833 (1954)
71. J. Haines, J.M. Léger, G. Bocquillon, Ann. Rev. Mater. Res. **31**, 1 (2001)
72. K. Nouneh, A.H. Reshak, S. Auluck, I.V. Kityk, R. Viennois, S. Benet, S. Charar, J. Alloys Compd. **437**, 39–46 (2007)

73. S. Berri, Comput. Cond. Matter **29**, e00595 (2021)
74. S. Berri, Comput. Cond. Matter **28**, e00586 (2021)
75. B. Ryu, M.-W. Oh, Computational simulations of thermoelectric transport properties. J. Korean Ceram. Soc. **53**, 273 (2016)
76. GS. Nolas, J. Sharp, and HJ. Goldsmid, Thermoelectrics: basic principles and new materials developments. Springer, Heidelberg, 2001.